Am J Transl Res 2026;18(8):6483-6504
www.ajtr.org /ISSN:1943-8141/AJTR0173828

Original Article

Harmine suppresses the malignant phenotypes of Lewis lung carcinoma cells by inhibiting EGFR phosphorylation

Xueliang Zhang[1,2*], Tao Wang[3*], Yonghua Hu[4], Caihong Fu[5,6], Xiaowen Lian[7], Yan Li[8], Ruoyu Zhao[1,2]

[1]Department of Gastrointestinal Medical Oncology, Sun Yat-sen University Cancer Center Gansu Hospital, Lanzhou 730050, Gansu, China; [2]Department of Gastrointestinal Medical Oncology, Gansu Provincial Cancer Hospital, Lanzhou 730050, Gansu, China; [3]Research Center of Translational Medicine, Gansu Provincial Academic Institute for Medical Research, Lanzhou 730050, Gansu, China; [4]The First Clinical Medical College and The Second Affiliated Hospital (Affiliated Hospital of Gansu University of Chinese Medicine), Gansu University of Chinese Medicine, Lanzhou 730099, Gansu, China; [5]Department of Thoracic Medical Oncology, Gansu Provincial Cancer Hospital, Lanzhou 730050, Gansu, China; [6]Department of Thoracic Medical Oncology, Sun Yat-sen University Cancer Center Gansu Hospital, Lanzhou 730050, Gansu, China; [7]Department of Medicine Biotechnology, Gansu Provincial Academic Institute for Medical Research, Lanzhou 730050, Gansu, China; [8]The First Clinical Medical College, Gansu University of Chinese Medicine, Lanzhou 730099, Gansu, China. [*]Equal contributors.

Received May 6, 2026; Accepted July 28, 2026; Epub August 15, 2026; Published August 30, 2026

Abstract: Objective: To investigate whether harmine (HM) suppresses the malignant phenotypes of Lewis lung carcinoma (LLC) cells through an epidermal growth factor receptor (EGFR) -mediated mechanism. Methods: Possible targets of HM and LLC-related genes were obtained from public databases, and overlapping targets were identified. A protein-protein interaction (PPI) network was constructed, followed by Gene Ontology (GO) and Kyoto Encyclopedia of Genes and Genomes (KEGG) enrichment analyses. Molecular docking was performed to predict the binding mode of HM with EGFR. The expression of phosphorylated EGFR (p-EGFR) was examined in LLC cells. *In vitro* assays were used to evaluate the effects of HM on cell viability, proliferation, colony formation, migration, invasion, and apoptosis. EGFR overexpression was further applied to assess whether EGFR was involved in the effects of HM. Results: A total of 121 overlapping targets between HM and LLC were identified, and EGFR was recognized as a core hub target in the PPI network. Molecular docking predicted that HM could fit into the ATP-binding pocket of EGFR, with a binding energy below -7.0 kcal/mol. In LLC cells, HM showed selective cytotoxicity and significantly inhibited EGFR phosphorylation. HM also reduced cell proliferation, colony formation, migration, and invasion, while promoting apoptosis. These effects were partially reversed by EGFR overexpression. Conclusion: HM suppresses the malignant phenotypes of LLC cells, at least in part, by inhibiting EGFR phosphorylation and EGFR-mediated signaling.

Keywords: Harmine, Lewis lung carcinoma, EGFR, bioinformatics, molecular docking

Introduction

Lung cancer is one of the most common and lethal malignancies worldwide. It remains a major threat to human health and a substantial global public health burden. According to recent global cancer statistics, both the incidence and mortality of lung cancer remain high, underscoring a need for more effective therapeutic strategies [1, 2]. Among the pathologic subtypes of lung cancer, non-small cell lung cancer (NSCLC) accounts for approximately 85% of all cases. NSCLC is characterized by insidious onset, rapid progression, and poor prognosis. Early symptoms are often atypical, and many patients are diagnosed at an advanced stage, when curative treatment options are limited. Therefore, further investigation of the molecular mechanisms underlying lung cancer progression is essential for improving therapeutic outcome.

Lewis lung carcinoma (LLC) is a widely used murine lung carcinoma model. It can mimic several key features of tumor growth, invasion, and metastatic dissemination *in vivo*. Because of these properties, LLC cells and LLC-bearing mouse models are extensively used in studies

https://doi.org/10.62347/ADGG4122

of lung cancer biology, anti-tumor drug screening, and tumor immunotherapy [3]. This model provides a useful experimental platform for evaluating candidate compounds and exploring their mechanisms of action.

Harmine (HM) is a β-carboline alkaloid derived from natural medicinal plants. It has diverse biological activities and has attracted increasing attention in cancer research [4-7]. Previous studies have shown that HM can exert anti-tumor effects through multiple mechanisms, including induction of tumor cell apoptosis [8, 9], inhibition of cell proliferation [10, 11], suppression of angiogenesis [12], regulation of the tumor immune microenvironment [13], and modulation of cell-cycle progression [14, 15]. HM has also shown anti-tumor activity in several tumor cell lines and animal models, with relatively low toxicity toward normal cells in some experimental settings [16-19]. However, its mechanism of action in LLC remains incompletely understood. In particular, the key molecular targets responsible for its inhibitory effects on LLC cells have not been fully clarified.

Epidermal growth factor receptor (EGFR) is a receptor tyrosine kinase that plays an important role in cell proliferation, differentiation, survival, and migration [20]. Under physiologic conditions, EGFR activation is tightly regulated. Ligand binding induces receptor dimerization and autophosphorylation, which subsequently activates downstream signaling pathways, including the RAS-RAF-MEK-ERK pathway [21, 22] and the PI3K-AKT-mTOR pathway [23-26]. These pathways coordinate multiple biological processes that are essential for normal cell function.

In many tumors, however, EGFR is overexpressed or aberrantly activated [27]. Persistent EGFR signaling promotes tumor cell proliferation, survival, migration, invasion, immune escape, and resistance to apoptosis [28-30]. For this reason, EGFR has become one of the most important therapeutic targets in lung cancer and other carcinomas. EGFR-targeted therapies, including small-molecule tyrosine kinase inhibitors and monoclonal antibodies, have achieved substantial clinical benefit in selected patients [31-37]. Nevertheless, drug resistance and heterogeneous therapeutic responses remain major challenges. New compounds that modulate EGFR-related signaling may therefore provide additional opportunities for anti-tumor intervention.

Given the reported anti-tumor potential of HM and the central role of EGFR in lung cancer progression, the present study investigated whether HM inhibits the malignant phenotypes of LLC cells through an EGFR-mediated mechanism. To address this question, we integrated bioinformatic analysis, protein-protein interaction network construction, functional enrichment analysis, molecular docking, and *in vitro* cellular assays. We further used EGFR overexpression to evaluate whether EGFR participates in the inhibitory effects of HM. This study may provide new mechanistic insight into the anti-tumor activity of HM and support its further preclinical evaluation as a candidate compound for lung cancer therapy.

Materials and methods

Bioinformatics analysis

Collection of potential target genes of harmine: The two-dimensional molecular structure of harmine (HM) was retrieved from PubChem. The structure was then submitted to three target prediction platforms, including PharmMapper, SwissTargetPrediction, and the Similarity Ensemble Approach (SEA). The species was set as *Mus musculus* when applicable. For PharmMapper, targets with a normalized fit score greater than 0.7 were retained. For SwissTargetPrediction, targets with a probability value greater than 0.1 were selected. For SEA, predicted targets were obtained using the default parameters of the platform. The predicted targets from all databases were merged, and duplicate entries were removed to generate a list of potential HM-related target genes.

Collection Lewis lung carcinoma-related target genes: Lewis lung carcinoma (LLC)-related genes were collected from GeneCards, the Comparative Toxicogenomics Database (CTD), and Online Mendelian Inheritance in Man (OMIM) using “Lewis Lung Carcinoma” and “Lung Neoplasms” as search terms. In GeneCards, genes with a relevance score greater than 10 were retained. In CTD and OMIM, genes directly associated with lung cancer etiology, progression, or pathologic processes were selected. The genes obtained from the three databases were then combined, and

duplicate entries were removed to construct the LLC-related target gene set. To match the mouse species setting used for HM target prediction, all human gene symbols obtained from the disease databases were mapped to their corresponding mouse orthologs using the R package biomaRt (Ensembl orthology database). After mapping, only genes with one-to-one orthologous relationships between human and mouse were retained, while genes without valid mouse homologs were excluded. The resulting set of mouse orthologs was defined as the final LLC-related gene set for subsequent bioinformatic analyses.

Identification of overlapping targets: The overlapping targets between the HM-related target set and the LLC-related target set were identified using the VennDiagram package in R. A Venn diagram was generated to visualize the intersection between the two target sets. These overlapping genes were considered candidate targets through which HM may exert biological effects on LLC cells.

Construction of protein-protein interaction network and identification of hub targets: The overlapping target genes were submitted to the STRING database version 12.0 for protein-protein interaction (PPI) analysis. The species was set as *Mus musculus*, and the minimum required interaction score was set to greater than 0.70. Disconnected nodes were hidden. The interaction data were exported in tab-separated values format and imported into Cytoscape for network visualization and topological analysis. Hub genes were identified using the CytoHubba plugin. Three topological algorithms, including Degree, Betweenness, and Closeness, were applied. The top 10 genes ranked by each algorithm were extracted, and their intersection was defined as the final set of core targets.

Gene ontology and Kyoto encyclopedia of genes and genomes enrichment analyses: Gene Ontology (GO) functional enrichment analysis and Kyoto Encyclopedia of Genes and Genomes (KEGG) pathway enrichment analysis were performed using the clusterProfiler package in R. GO analysis included three categories: biological process (BP), cellular component (CC), and molecular function (MF). Enriched terms or pathways with an adjusted *P* value less than 0.05 and an enrichment factor greater than 1.5 were considered significant.

Construction of the drug-target-pathway network: Information on HM, core overlapping targets, and significantly enriched KEGG pathways was integrated to construct a drug-target-pathway network. Node and edge files were prepared and imported into Cytoscape for visualization. In this network, HM, core targets, and enriched pathways were represented as nodes, while their associations were represented as edges. This network was used to illustrate the potential multi-target and multi-pathway mechanisms by which HM may affect LLC cells.

Molecular docking

Molecular docking was performed to predict the potential binding mode between HM and EGFR. The crystal structure of EGFR was obtained from the Protein Data Bank (PDB ID: 1M17). The receptor protein was prepared by removing water molecules and original ligands. The three-dimensional structure of HM was retrieved from PubChem and optimized by hydrogenation and charge assignment.

The docking grid was centered on the ATP-binding pocket of the EGFR kinase domain. Semi-flexible docking was performed using AutoDock Vina. The conformation with the lowest predicted binding free energy was selected for further analysis. The binding pose and intermolecular interactions were visualized using PyMOL.

Cell experiments

Cell culture: The mouse Lewis lung carcinoma cell line LL/2 (LLC1), the human normal lung epithelial cell line BEAS-2B, the human non-small cell lung cancer cell line A549, and the normal mouse lung epithelial cell line MLE-12 were purchased from the Cell Resource Center of the Shanghai Institute of Life Sciences, Chinese Academy of Sciences. LLC1, BEAS-2B, and MLE-12 cells were cultured in Dulbecco's modified Eagle's medium (DMEM; Gibco, Thermo Fisher Scientific, USA) supplemented with 10% fetal bovine serum and 1% penicillin-streptomycin. A549 cells were cultured in RPMI-1640 medium (Catalog No.: 11875093, Gibco, Thermo Fisher Scientific, USA) supplemented with 10% FBS and 1%

penicillin-streptomycin. All cells were maintained at 37°C in a humidified incubator containing 5% CO_2.

Reagents and antibodies: HM was purchased from Shanghai Yuanye Bio-Technology Co., Ltd. and dissolved in dimethyl sulfoxide to prepare a 50 mM stock solution, which was stored at -20°C. Cell Counting Kit-8 (CCK-8), 5-ethynyl-2'-deoxyuridine (EdU) proliferation kit, Transwell chambers, Matrigel, TUNEL apoptosis detection kit, RIPA lysis buffer, and BCA protein assay kit were used according to the manufacturers' instructions.

Additional primary antibodies used for western blotting and immunofluorescence analysis included rabbit anti-phospho-AKT (Ser473) (Cat. No. 4060T), rabbit anti-pan-AKT (Cat. No. 4691T), rabbit anti-phospho-ERK1/2 (Thr202/Tyr204) (Cat. No. 4370T), rabbit anti-total ERK1/2 (Cat. No. 4695T), rabbit anti-p-EGFR (Tyr1068), and rabbit anti-total EGFR monoclonal antibodies, all purchased from Cell Signaling Technology (Danvers, MA, USA). Rabbit anti-cleaved caspase-3 polyclonal antibody (Cat. No. 25128-1-PBS) and mouse anti-GAPDH monoclonal antibody (Cat. No. 60004-1-Ig) were obtained from Proteintech Group (Wuhan, China). Appropriate horseradish peroxidase-conjugated or fluorescence-conjugated secondary antibodies were used for signal detection. DAPI was used for nuclear counterstaining.

EGFR overexpression: Cells were transfected with a mouse EGFR overexpression plasmid or the corresponding empty vector using Lipofectamine 3000. Forty-eight hours after transfection, cells were selected with puromycin to establish stable EGFR-overexpressing cells (OE-EGFR) and negative control cells (NC).

Western blotting: Total cellular proteins were extracted using RIPA lysis buffer and quantified using the BCA method. Equal amounts of protein were separated by SDS-PAGE and transferred onto polyvinylidene fluoride membranes. After blocking with 5% skim milk, the membranes were incubated with primary antibodies overnight at 4°C, followed by incubation with secondary antibodies at room temperature. Protein bands were detected using an enhanced chemiluminescence substrate and visualized with a ChemiDoc imaging system. GAPDH was used as the internal loading control.

Cell viability, proliferation, migration, invasion, and apoptosis assays: To determine the optimal HM concentration and evaluate selective cytotoxicity, cells were seeded into 96-well plates at 5×10^3 cells per well and treated with HM at 0, 2.5, 5, 10, 20, 40, or 80 μM for 24 h. Cell viability was assessed using the CCK-8 assay, and absorbance was measured at 450 nm. The IC_{50} value was calculated by nonlinear regression using GraphPad Prism 9.0. The selectivity index was calculated as the ratio of BEAS-2B cell viability to LLC and A549 cells viability at each HM concentration.

For functional assays, cells were divided into four groups: NC, HM, OE-EGFR, and OE-EGFR+HM. Cells in the HM and OE-EGFR+HM groups were treated with 20 μM HM, whereas the NC and OE-EGFR groups received vehicle control. Cell proliferation was assessed using CCK-8 and EdU assays. For the CCK-8 assay, cells were seeded into 96-well plates at 5×10^3 cells per well. After 24 h of attachment, cells were treated with the corresponding drugs as described above. Cell viability was measured at 0, 24, and 48 h after treatment by adding 10 μL of CCK-8 solution to each well, followed by incubation at 37°C for 2 h. The absorbance was then recorded at 450 nm using a microplate reader. For the EdU assay, cells were incubated with 10 μM EdU for 2 h, followed by click reaction and nuclear staining according to the manufacturer's instructions. The proportion of EdU-positive cells was calculated from at least five randomly selected fields. Cell migration was evaluated using a wound healing assay. Cells were seeded into 6-well plates and cultured until they reached more than 90% confluence. A linear scratch was generated using a sterile 200 μL pipette tip. Detached cells were removed with phosphate-buffered saline, and cells were cultured in serum-free medium with the indicated treatments. Images were captured at 0, 24, and 48 h, and wound closure was quantified using ImageJ. Cell invasion was assessed using Matrigel-coated Transwell chambers. A total of 5×10^4 cells suspended in serum-free medium were added to the upper chamber, while medium containing 10% fetal bovine serum was added to the lower chamber as a chemoattrac-

tant. After 48 h, non-invading cells were removed. Invaded cells were fixed with 4% paraformaldehyde, stained with 0.1% crystal violet, and counted under a light microscope in five randomly selected fields. Cell apoptosis was detected using a TUNEL apoptosis detection kit according to the manufacturer's protocol. Nuclei were counterstained with DAPI, and TUNEL-positive cells were quantified under a fluorescence microscope.

Colony formation assay: Cells in the logarithmic growth phase were seeded into 6-well plates at 500 cells per well. After attachment, cells were treated according to the four experimental groups: NC, HM, OE-EGFR, and OE-EGFR+HM. The HM-containing groups received 20 μM HM. Cells were cultured for 10-14 days, and the medium was replaced every 3 days. Colonies were fixed with 4% paraformaldehyde and stained with 0.1% crystal violet. Colonies containing more than 50 cells were counted under a light microscope. Relative colony formation efficiency was calculated as the number of colonies in each treatment group divided by the number of colonies in the NC group × 100%.

Statistical analysis

All experiments were performed independently at least three times. Data were presented as mean ± standard deviation (SD). Statistical analyses were performed using GraphPad Prism 9.0 software (GraphPad Software, San Diego, CA, USA). For comparisons between two groups, unpaired two-tailed Student's t-test was used. For comparisons involving multiple groups, one-way analysis of variance (ANOVA) followed by Tukey's post-hoc test was applied. ImageJ software (National Institutes of Health, Bethesda, MD, USA) was used for quantification of western blot band intensities, EdU-positive cell percentages, wound healing areas, and cell counts in invasion and colony formation assays. For western blotting, band intensities were normalized to GAPDH as the loading control. For EdU staining, the percentage of EdU-positive cells was calculated as (EdU-positive cells/total cells) × 100%. For wound healing assays, the migration rate was calculated as [(wound area at 0 h - wound area at indicated time)/wound area at 0 h] × 100%. For IHC, the p-EGFR-positive rate was calculated as (p-EGFR-positive cells/total cells counted) × 100%. A P-value < 0.05 was considered significant. Significance levels are indicated as $P < 0.05$, $*P < 0.01$, and $**P < 0.001$.

Results

Target screening identifies EGFR as a candidate hub target of HM in LLC

To explore the potential molecular targets involved in the inhibitory effects of HM on LLC cells, target prediction and disease-gene mining were first integrated. Candidate HM-related targets were predicted using multiple target prediction platforms. As shown in **Figure 1A**, different platforms generated partially overlapping target sets, indicating both consistency and complementarity among the prediction results.

LLC-related genes were then collected from disease-associated databases, including OMIM, GeneCards, and CTD. Venn analysis showed that 75 genes were shared among these disease-related datasets, suggesting that the collected gene set was relatively reliable for subsequent analysis (**Figure 1B**). The predicted HM-related targets were further intersected with LLC-related genes. A total of 121 overlapping genes were identified and considered candidate targets through which HM may affect LLC cells (**Figure 1C**).

To identify key targets among these candidates, the 121 overlapping genes were subjected to protein-protein interaction (PPI) network analysis. The resulting network revealed several highly connected nodes, including EGFR, SRC, and CASP3 (**Figure 1D**). Among them, EGFR occupied a central position and showed extensive interactions with other candidate targets (**Figure 1E**). These findings suggest that EGFR may be an important hub target involved in the possible anti-LLC activity of HM.

Functional enrichment analysis suggests the involvement of EGFR-related signaling in the effects of HM on LLC

To further characterize the biological functions of the overlapping targets, GO and KEGG enrichment analyses were performed. GO enrichment analysis showed that the overlapping targets were mainly associated with protein phosphorylation-related biological processes, including peptidyl-serine phosphorylation and protein autophosphorylation (**Figure 2A**). These

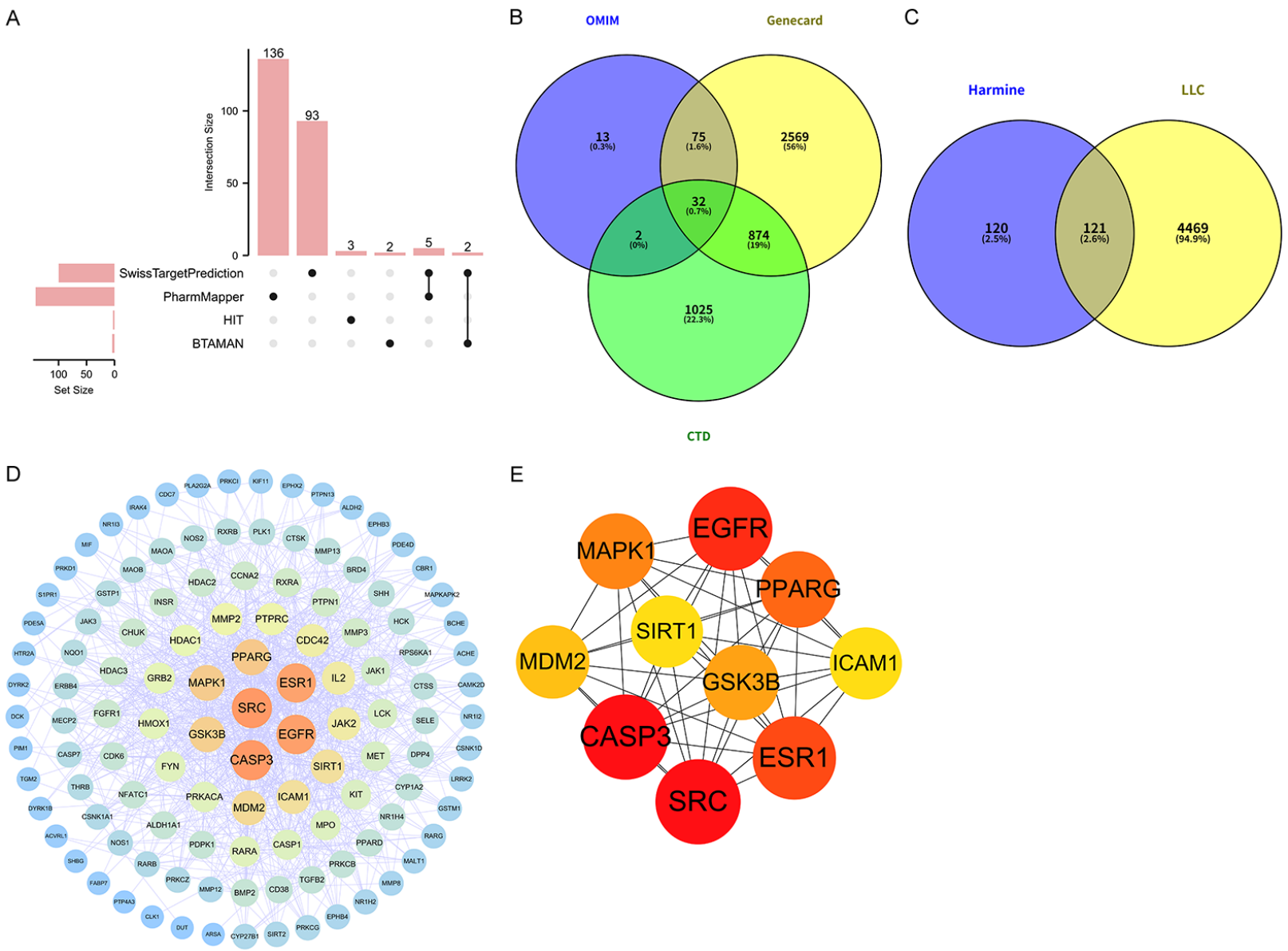

Figure 1. Target screening identifies EGFR as a candidate hub target of HM in LLC. A. Comparison of predicted HM-related targets obtained from different target prediction platforms. B. Venn diagram showing the overlap among LLC-related genes retrieved from OMIM, GeneCards, and CTD. C. Venn diagram showing the intersection between predicted HM-related targets and LLC-related genes. A total of 121 overlapping genes were identified as candidate targets. D. Protein-protein interaction network of the 121 overlapping targets. Larger nodes indicate higher network connectivity. E. Subnetwork centered on EGFR and its interacting proteins.

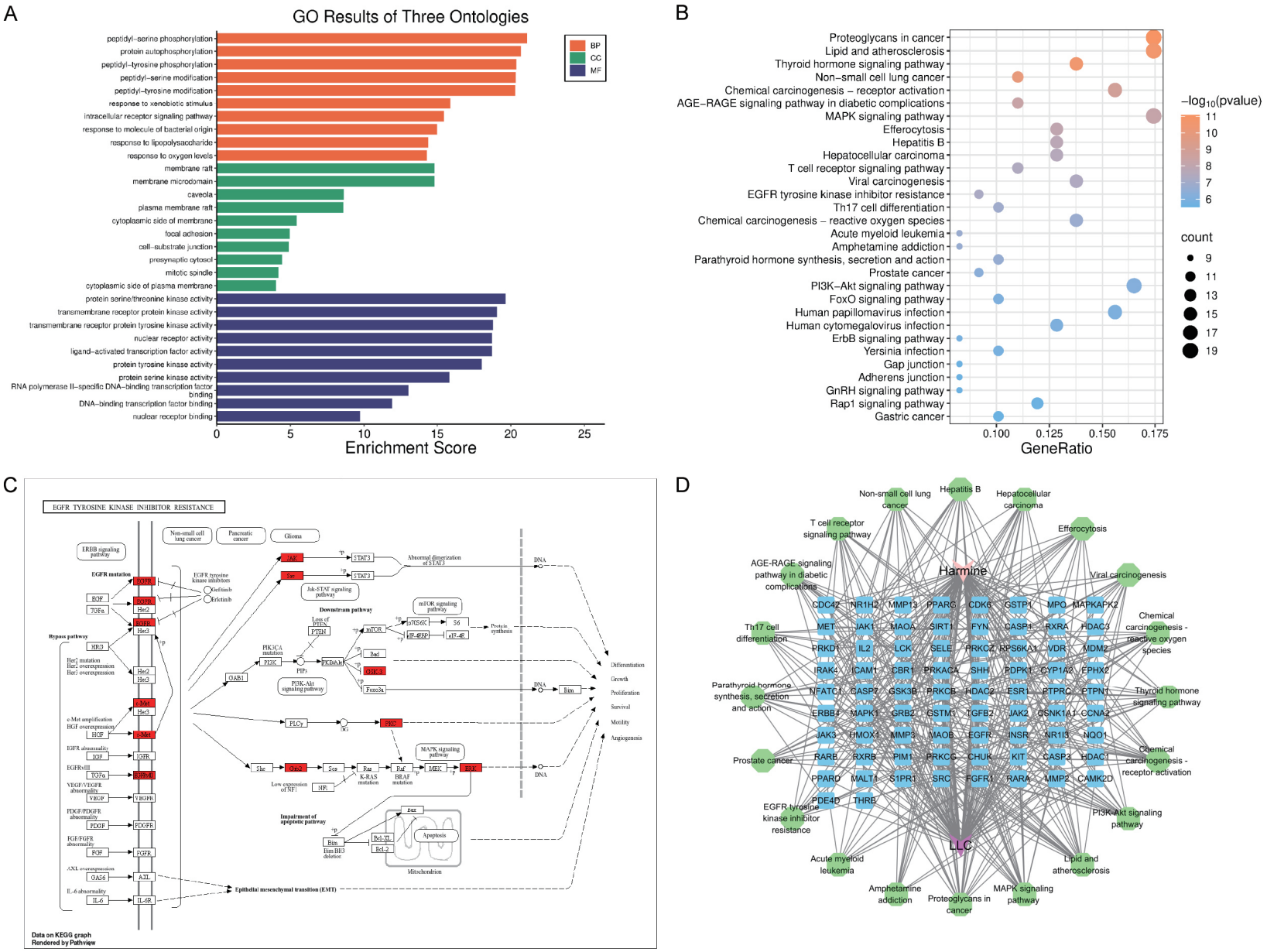
A
GO Results of Three Ontologies
peptidyl−serine phosphorylation
protein autophosphorylation
peptidyl−tyrosine phosphorylation
peptidyl−serine modification
peptidyl−tyrosine modification
response to xenobiotic stimulus
intracellular receptor signaling pathway
response to molecule of bacterial origin
response to lipopolysaccharide
response to oxygen levels
membrane raft
membrane microdomain
caveola
plasma membrane raft
cytoplasmic side of membrane
focal adhesion
cell−substrate junction
presynaptic cytosol
mitotic spindle
cytoplasmic side of plasma membrane
protein serine/threonine kinase activity
transmembrane receptor protein kinase activity
transmembrane receptor protein tyrosine kinase activity
nuclear receptor activity
ligand−activated transcription factor activity
protein tyrosine kinase activity
protein serine kinase activity
RNA polymerase II−specific DNA−binding transcription factor binding
DNA−binding transcription factor binding
nuclear receptor binding
BP
CC
MF
0
5
10
15
20
25
Enrichment Score
B
Proteoglycans in cancer
Lipid and atherosclerosis
Thyroid hormone signaling pathway
Non−small cell lung cancer
Chemical carcinogenesis − receptor activation
AGE−RAGE signaling pathway in diabetic complications
MAPK signaling pathway
Efferocytosis
Hepatitis B
Hepatocellular carcinoma
T cell receptor signaling pathway
Viral carcinogenesis
EGFR tyrosine kinase inhibitor resistance
Th17 cell differentiation
Chemical carcinogenesis − reactive oxygen species
Acute myeloid leukemia
Amphetamine addiction
Parathyroid hormone synthesis, secretion and action
Prostate cancer
PI3K−Akt signaling pathway
FoxO signaling pathway
Human papillomavirus infection
Human cytomegalovirus infection
ErbB signaling pathway
Yersinia infection
Gap junction
Adherens junction
GnRH signaling pathway
Rap1 signaling pathway
Gastric cancer
0.100
0.125
0.150
0.175
GeneRatio
−log10(pvalue)
11
10
9
8
7
6
count
9
11
13
15
17
19
C
EGFR TYROSINE KINASE INHIBITOR RESISTANCE
Data on KEGG graph
Rendered by Pathview
D
Harmine
LLC
Non−small cell lung cancer
Hepatitis B
Hepatocellular carcinoma
T cell receptor signaling pathway
Efferocytosis
AGE−RAGE signaling pathway in diabetic complications
Viral carcinogenesis
Th17 cell differentiation
Chemical carcinogenesis − reactive oxygen species
Parathyroid hormone synthesis, secretion and action
Thyroid hormone signaling pathway
Prostate cancer
Chemical carcinogenesis − receptor activation
EGFR tyrosine kinase inhibitor resistance
PI3K−Akt signaling pathway
Acute myeloid leukemia
Lipid and atherosclerosis
Amphetamine addiction
Proteoglycans in cancer
MAPK signaling pathway
CDC42
NR1H2
MMP13
PPARG
CDK6
GSTP1
MPO
MAPKAPK2
MET
JAK1
MAOA
SIRT1
FYN
CASP8
RXRA
HDAC3
PRKD1
IL2
LCK
SELE
PRKC2
RPS6KA1
VDR
MDM2
IRAK4
ICAM1
CBR1
PRKACA
SHH
PDPK1
CYP1A2
EPHX2
NFATC1
CASP7
GSK3B
PRKCB
HDAC2
ESR1
PTPRC
PTPNT
ERBB4
MAPK1
GRB2
GSTM1
TGFB2
JAK2
CSNK1A1
CCNA2
JAK3
HMOX1
MMP3
MAOB
EGFR
INSR
NR1I3
NQO1
RARB
RXRB
PIM1
PRKCG
CHUK
KIT
CASP3
HDAC1
PPARD
MALT1
S1PR1
SRC
FGFR1
RARA
MMP2
CAMK2D
PDE4D
THRB

Figure 2. Functional enrichment analysis and drug-target-pathway network of HM-related candidate targets in LLC. A. Gene Ontology enrichment analysis of the overlapping targets, including biological process, cellular components, and molecular function categories. B. Kyoto Encyclopedia of Genes and Genomes pathway enrichment analysis of the overlapping targets. C. EGFR tyrosine kinase inhibitor resistance pathway map showing the distribution of candidate targets within EGFR-related signaling cascades. D. Drug-target-pathway network integrating HM, core overlapping targets, and enriched pathways.

processes are closely related to receptor tyrosine kinase activation and downstream signal transduction.

In the cellular component category, enriched terms were mainly associated with membrane rafts and the plasma membrane. This finding suggests that membrane-associated signaling events may be involved in the effects of HM on LLC cells. In the molecular function category, several enriched terms were related to transmembrane receptor protein tyrosine kinase activity, which is consistent with the central position of EGFR identified in the PPI network.

KEGG pathway enrichment analysis further showed that the overlapping targets were enriched in several cancer-related pathways, including pathways in cancer, proteoglycans in cancer, the thyroid hormone signaling pathway, non-small cell lung cancer, and the EGFR tyrosine kinase inhibitor resistance pathway (**Figure 2B**). These enriched pathways indicated that the candidate targets of HM were closely associated with oncogenic signaling networks. In particular, the enrichment of EGFR-related pathways supports EGFR as a plausible mechanistic target for further validation.

A pathway map of EGFR tyrosine kinase inhibitor resistance was used to display the distribution of candidate targets within EGFR-related signaling cascades (**Figure 2C**). In addition, a drug-target-pathway network was constructed to integrate HM, core overlapping targets, and enriched KEGG pathways (**Figure 2D**). This network further suggested that HM may affect LLC cells through a multi-target and multi-pathway mechanism, with EGFR serving as a key candidate hub.

Molecular docking predicts a potential binding mode between HM and EGFR

Based on the pathway and network analyses, EGFR was selected for molecular docking to further explore its potential interaction with HM. The docking results predicted that HM could fit into the ATP-binding pocket of the EGFR kinase domain. The predicted binding energy was less than -7.0 kcal/mol, suggesting a relatively stable binding conformation.

As shown in **Figure 3A**, HM was located within the active pocket of EGFR. The compound was stabilized mainly by hydrophobic interactions and π-π stacking. Key residues, including PHE99, VAL36, LEU115, and VAL85, were involved in maintaining the ligand-receptor complex. The two-dimensional interaction diagram further showed that π-π stacking and alkyl/π-alkyl interactions contributed to the predicted binding mode between HM and EGFR (**Figure 3B**).

These docking results suggest that HM may interact with the ATP-binding region of EGFR where it can interfere with EGFR kinase activation. This structural prediction provided a rationale for subsequent experimental validation of EGFR phosphorylation in LLC cells.

EGFR is constitutively activated in LLC cells and suppressed by HM

To confirm that EGFR exhibits constitutive abnormal activation in murine LLC lung tumor cells at the cellular level, we compared the baseline expression of EGFR and p-EGFR between normal mouse lung epithelial MLE-12 cells and untreated LLC cells by western blot (**Figure 4A**). The quantitative results revealed that total EGFR protein showed no obvious difference between MLE-12 and LLC cells (ns), while the phosphorylation level of EGFR was markedly higher in LLC cells than that in normal MLE-12 cells ($P < 0.05$). In addition, stimulation with exogenous EGF further robustly upregulated p-EGFR abundance in LLC cells ($P < 0.01$). These data provide direct cellular evidence that EGFR signaling is inherently hyperactivated in LLC tumor cells compared to normal pulmonary epithelial cells, laying a core prerequisite for our subsequent HM intervention and EGFR rescue assays.

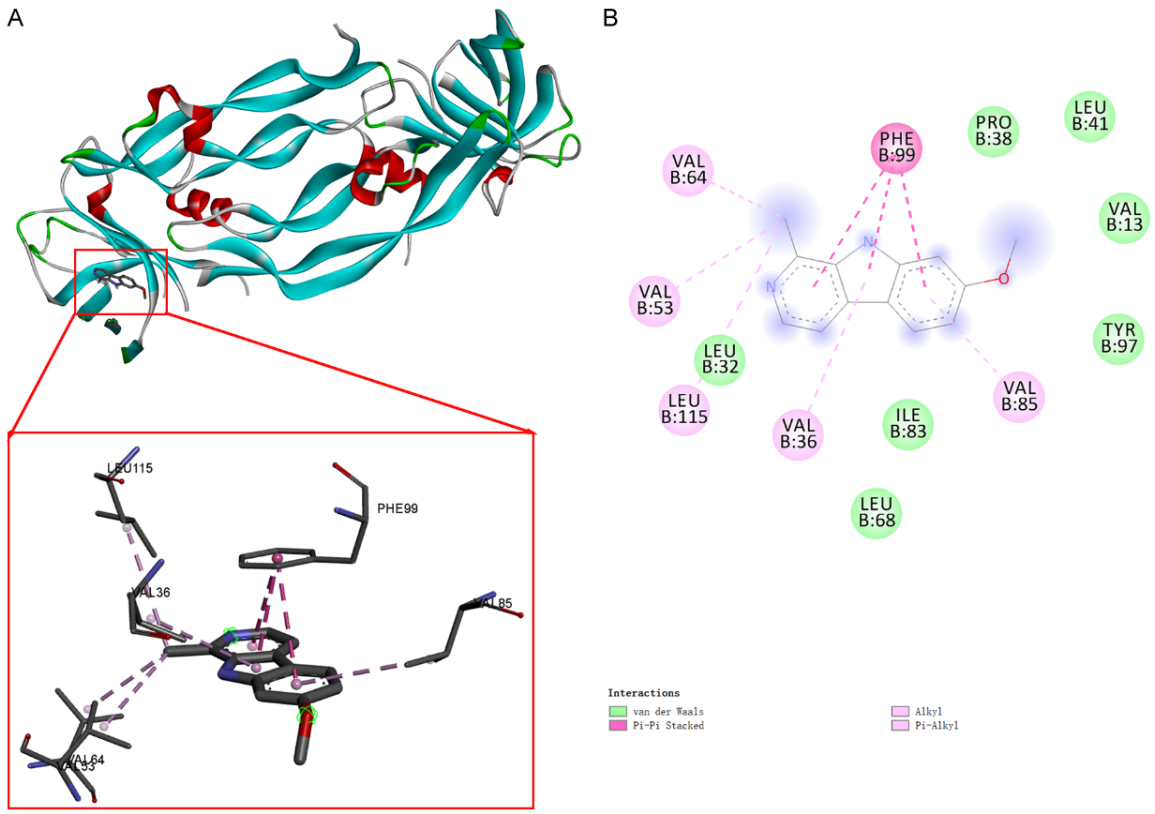

Figure 3. Molecular docking analysis of the predicted interaction between HM and EGFR. A. Three-dimensional binding conformation of HM within the ATP-binding pocket of the EGFR kinase domain. B. Two-dimensional interaction diagram showing the predicted intermolecular interactions between HM and EGFR, including hydrophobic interactions, π-π stacking, and alkyl/π-alkyl interactions.

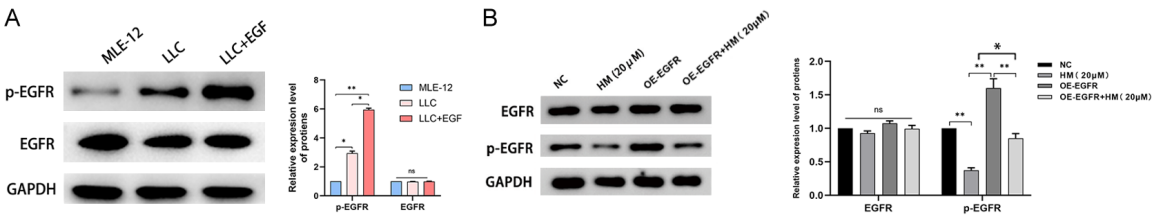

Figure 4. EGFR is constitutively activated in LLC cells and suppressed by HM. A. Western blot analysis of EGFR and p-EGFR protein levels in MLE-12 and LLC cells after treatments. B. Western blot analysis of EGFR and p-EGFR protein levels in LLC cells under four different treatments: NC, HM (20 μM), OE-EGFR, and OE-EGFR+HM (20 μM). HM reduced p-EGFR expression without significantly altering total EGFR expression, and EGFR overexpression partially attenuated this effect. ns, not significant; $P < 0.05$; *$P < 0.01$; **$P < 0.001$.

To determine whether HM inhibits aberrant EGFR activation in LLC cells, LLC cells were subjected to 20 μM HM treatment and subjected to western blot detection (**Figure 4B**). HM treatment significantly reduced p-EGFR levels relative to the NC blank control group ($P < 0.001$), while the total protein abundance of EGFR remained unchanged with no statistical difference. This observation suggests that HM represses EGFR signaling mainly through blocking EGFR phosphorylation, rather than downregulating total EGFR protein expression.

EGFR overexpression markedly increased p-EGFR levels compared to the NC group ($P < 0.01$). In the OE-EGFR+HM co-treatment group, p-EGFR levels were significantly restored compared to the HM single treatment group ($P < 0.01$), yet remained distinctly lower than those of the NC blank control group ($P < 0.01$). These

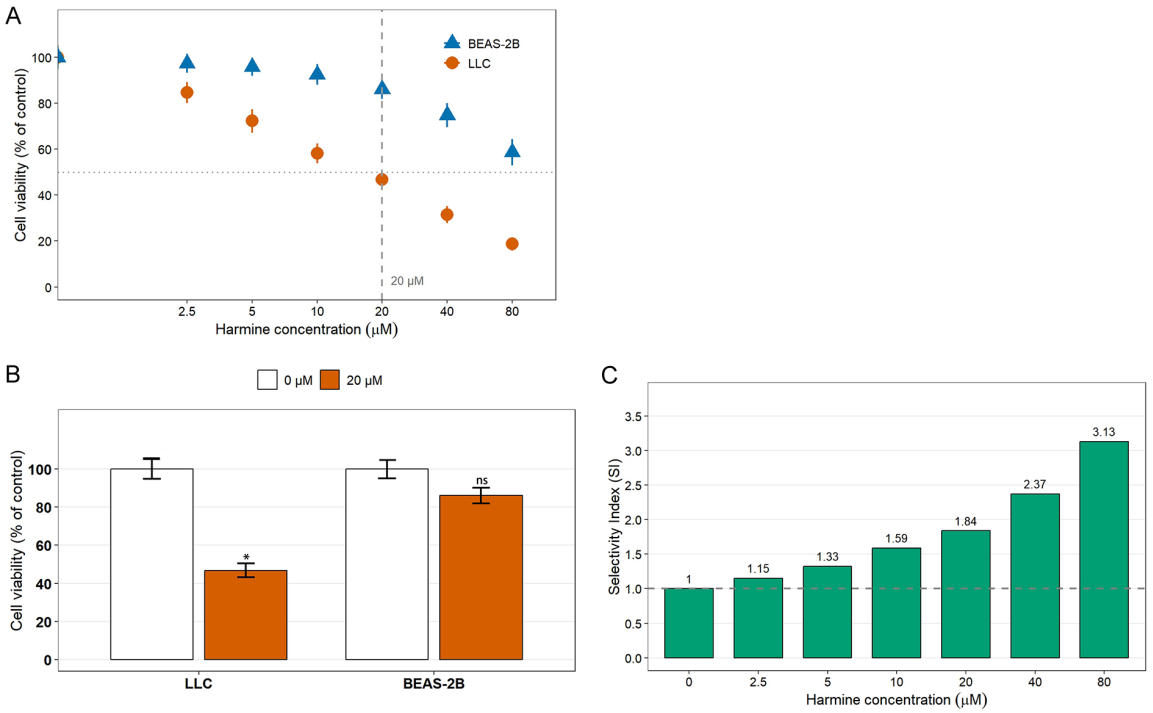

Figure 5. Dose-response cytotoxicity of HM in LLC and BEAS-2B cells. A. LLC and BEAS-2B cells were treated with increasing concentrations of HM from 0 to 80 μM for 24 h, and cell viability was assessed using the CCK-8 assay. The IC_{50} value of HM in LLC cells was 19.1 ± 3.5 μM. B. Comparison of cell viability between LLC and BEAS-2B cells after treatment with 20 μM HM. C. Selectivity index of HM at different concentrations. The selectivity index was calculated as BEAS-2B cell viability divided by LLC cell viability. Data are presented as the mean ± SD from three independent experiments. ****P < 0.001*; ns, not significant.

results indicate that EGFR overexpression only partially attenuated HM-mediated inhibition of EGFR phosphorylation and could not fully restore EGFR activation to the baseline level of untreated normal LLC cells. Together, these data systematically demonstrated that HM effectively suppresses the abnormally activated EGFR phosphorylation signaling in LLC tumor cells.

HM exhibits selective cytotoxicity against LLC cells

To determine the appropriate concentration of HM for subsequent functional assays, dose-response CCK-8 assays were performed in LLC cells and BEAS-2B normal lung epithelial cells. Cells were treated with different concentrations of HM ranging from 0 to 80 μM for 24 h, and cell viability was then assessed.

As shown in **Figure 5A**, HM reduced LLC cell viability in a concentration-dependent manner. The calculated IC_{50} value in LLC cells was approximately 19.1 ± 3.5 μM. Therefore, 20 μM HM was selected for subsequent experiments. At this concentration, LLC cell viability decreased to 46.8 ± 3.6% of the control level. In contrast, BEAS-2B cells retained 86.1 ± 4.2% viability after treatment with 20 μM HM, which was significantly higher than that of LLC cells (*P < 0.001*; **Figure 5B**).

The selectivity index, calculated as the ratio of BEAS-2B cell viability to LLC cell viability, was 1.84 at 20 μM HM. In addition, the selectivity index increased as the HM concentration increased (**Figure 5C**). These results indicated that HM exhibits greater cytotoxicity toward LLC cells than toward BEAS-2B cells *in vitro*, supporting the use of 20 μM HM in subsequent functional experiments.

HM suppresses downstream AKT and ERK1/2 signaling pathways in LLC cells

To determine whether HM-mediated inhibition of EGFR phosphorylation leads to suppression of downstream signaling cascades, we examined the phosphorylation status of AKT and

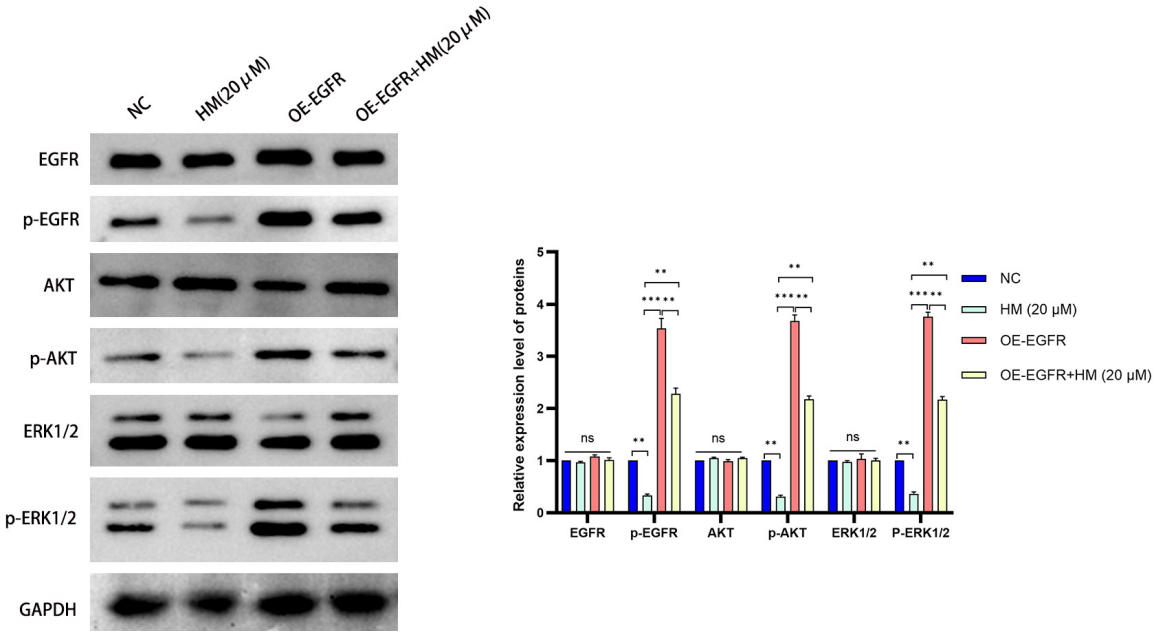

Figure 6. HM suppresses downstream AKT and ERK1/2 signaling pathways in LLC cells. Western blot analysis of p-EGFR (Tyr1068), total EGFR, p-AKT (Ser473), total AKT, p-ERK1/2 (Thr202/Tyr204), total ERK1/2 in LLC cells after different treatments. Data are presented as mean ± SD from three independent experiments. $^{**}P < 0.01$, $^{***}P < 0.001$; ns, not significant.

ERK1/2 by western blotting in LLC cells with or without EGFR overexpression. As shown in **Figure 6**, HM treatment (20 μM) significantly reduced the phosphorylation levels of both AKT (Ser473) and ERK1/2 (Thr202/Tyr204) compared to the NC group ($P < 0.01$), while total AKT and total ERK1/2 protein levels remained unchanged across all groups. Conversely, EGFR overexpression (EGFR) markedly increased p-AKT and p-ERK1/2 levels compared to the NC group ($P < 0.001$). Notably, when EGFR-overexpressing cells were co-treated with HM, the phosphorylation levels of both p-AKT and p-ERK1/2 were significantly reduced compared to the OE-EGFR group ($P < 0.01$), while remaining significantly higher than those in the HM (20 μM) group ($P < 0.01$), demonstrating a partial rescue effect. These results confirm that HM effectively suppressed both the PI3K-AKT and RAS-RAF-MEK-ERK signaling pathways downstream of EGFR in an EGFR-dependent manner.

HM inhibits LLC cell proliferation, colony formation, invasion, and migration in an EGFR-related manner

To determine whether HM affects the malignant phenotypes of LLC cells, proliferation, colony formation, invasion, and migration assays were performed. As shown in **Figure 7A**, EdU staining showed that HM treatment significantly reduced the proportion of EdU-positive cells compared with the NC group ($P < 0.05$). When EGFR-overexpressing cells were co-treated with HM (OE-EGFR+HM), the EdU-positive rate was significantly lower than that in the OE-EGFR group ($P < 0.05$), indicating that HM retained inhibitory activity even in the presence of EGFR overexpression. However, the EdU-positive rate in the OE-EGFR+HM group remained significantly higher than that in the HM group ($P < 0.05$), suggesting that EGFR overexpression partially attenuated the inhibitory effect of HM on cell proliferation. Notably, the OE-EGFR+HM group exhibited an EdU-positive rate lower than that of the NC group, further reflecting the potent anti-proliferative activity of HM.

Consistent results were obtained from the CCK-8 assay. HM significantly reduced LLC cell viability at 24 and 48 h compared to the NC group ($P < 0.05$), whereas EGFR overexpression significantly increased cell viability compared to the NC group ($P < 0.01$; **Figure 7B**). HM treatment also significantly reduced the viability of EGFR-overexpressing cells compared to

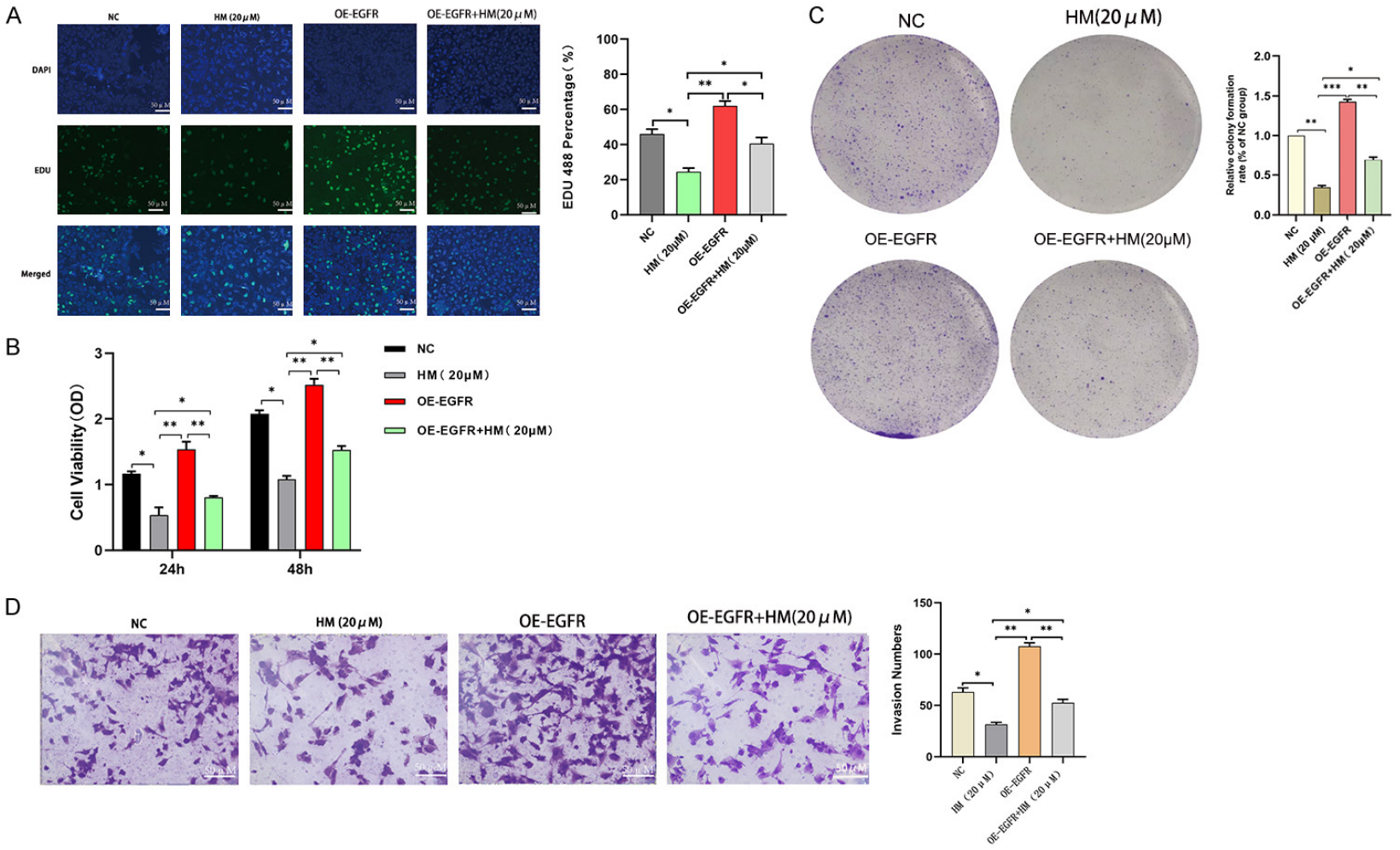
A
NC
HM (20 μM)
OE-EGFR
OE-EGFR+HM(20 μM)
DAPI
EDU
Merged
EDU 488 Percentage (%)
NC
HM (20μM)
OE-EGFR
OE-EGFR+HM(20μM)
B
Cell Viability (OD)
24h
48h
NC
HM (20μM)
OE-EGFR
OE-EGFR+HM (20μM)
C
NC
HM(20 μM)
OE-EGFR
OE-EGFR+HM(20μM)
Relative colony formation rate (% of NC group)
D
NC
HM (20 μM)
OE-EGFR
OE-EGFR+HM(20 μM)
Invasion Numbers

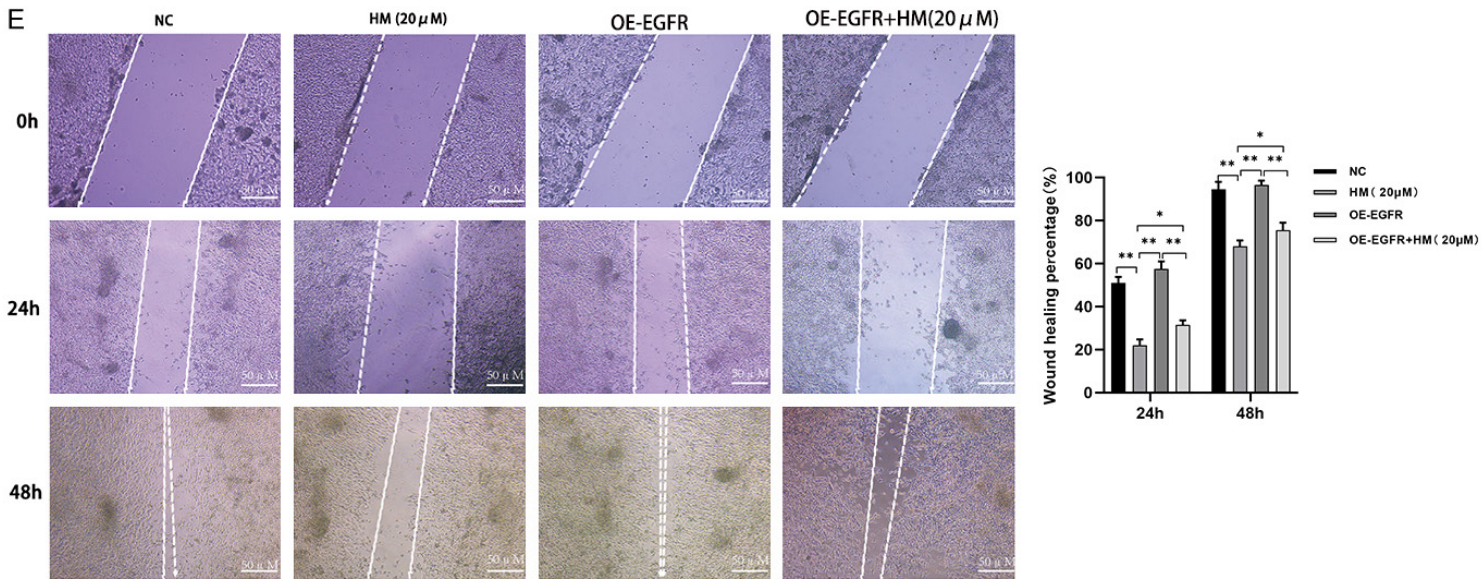

Figure 7. HM inhibits proliferation, colony formation, invasion, and migration of LLC cells in an EGFR-related manner. A. EdU staining assay showing the effect of HM and EGFR overexpression on LLC cell proliferation. B. CCK-8 assay showing LLC cell viability at 24 and 48 h after different treatments. C. Colony formation assay showing the long-term clonogenic capacity of LLC cells. D. Transwell invasion assay showing the invasive ability of LLC cells. E. Wound healing assay showing the migratory ability of LLC cells at 24 and 48 h. Data are presented as the mean ± SD from three independent experiments. *$P < 0.05$; **$P < 0.01$.

the OE-EGFR group ($P < 0.01$). However, the viability of the OE-EGFR+HM group remained significantly higher than that of the HM group at both 24 and 48 h ($P < 0.05$), indicating that EGFR overexpression partially counteracted the anti-proliferative effect of HM. These results further support the inhibitory effect of HM on LLC cell proliferation and the involvement of EGFR in mediating this effect.

The colony formation assay showed that HM markedly reduced both the number and size of colonies compared with the NC group ($P < 0.01$; **Figure 7C**). EGFR overexpression significantly promoted colony formation compared to the NC group ($P < 0.01$). HM treatment significantly suppressed colony formation in EGFR-overexpressing cells compared to the OE-EGFR group ($P < 0.05$). However, the colony number in the OE-EGFR+HM group remained significantly higher than that of the HM group ($P < 0.05$), confirming that EGFR overexpression partially rescued the clonogenic capacity. These data indicate that HM inhibits the long-term clonogenic capacity of LLC cells and may counteract the pro-proliferative effect of EGFR overexpression.

Next, Transwell and wound healing assays were used to evaluate cell invasion and migration. HM significantly decreased the number of invading cells compared to the NC group ($P < 0.05$), while EGFR overexpression enhanced invasion ($P < 0.01$; **Figure 7D**). In the OE-EGFR+HM group, the number of invading cells was significantly lower than that of the OE-EGFR group ($P < 0.01$). However, the invasive ability of the OE-EGFR+HM group remained significantly higher than that of the HM group ($P < 0.05$), indicating that EGFR overexpression partially rescued the invasive phenotype. Notably, the OE-EGFR+HM group showed an invasion level lower than that of the NC group, further reflecting the potent anti-invasive activity of HM. Similarly, wound healing assays showed that HM reduced wound closure at 24 and 48 h, whereas EGFR overexpression accelerated wound closure (**Figure 7E**). HM treatment significantly attenuated the EGFR overexpression-induced increase in migratory ability. However, the migration rate in the OE-EGFR+HM group remained significantly higher than that in the HM group ($P < 0.05$), suggesting that EGFR overexpression partially rescued the migratory capacity. These results collectively demonstrate that HM suppresses LLC cell migration in an EGFR-related manner.

Together, these results demonstrate that HM suppresses proliferation, colony formation, invasion, and migration of LLC cells. In all assays, EGFR overexpression significantly attenuated but did not abolish the inhibitory effects of HM, as evidenced by the consistent finding that OE-EGFR+HM group values were significantly higher than those of the HM group but significantly lower than those of the OE-EGFR group. These results confirm that the anti-malignant effects of HM are partially mediated through EGFR, while the sustained inhibition in the OE-EGFR+HM group suggests additional EGFR-independent contributions.

HM exerts similar inhibitory effects on proliferation, colony formation, invasion, and migration in human NSCLC A549 cells

To evaluate whether the inhibitory effects of HM observed in LLC cells could be generalized to human lung cancer and whether EGFR is similarly involved, we repeated the four-group functional assays in the human NSCLC A549 cell line.

As shown in **Figure 8A**, EdU staining demonstrated that HM treatment (20 μM) markedly decreased the proportion of proliferating A549 cells compared to the NC group ($P < 0.05$), consistent with the anti-proliferative effect observed in LLC cells. EGFR overexpression significantly increased the EdU-positive rate compared to the NC group ($P < 0.01$). When EGFR-overexpressing cells were co-treated with HM (OE-EGFR+HM), the EdU-positive rate was significantly lower than that in the OE-EGFR group ($P < 0.05$), indicating that HM retained inhibitory activity even in the presence of EGFR overexpression. However, the EdU-positive rate in the OE-EGFR+HM group remained significantly higher than that of the HM group ($P < 0.05$), suggesting that EGFR overexpression partially attenuated the inhibitory effect of HM on A549 cell proliferation.

Consistent results were obtained from the CCK-8 assay. HM significantly reduced A549 cell viability at 24 and 48 h compared to the NC group ($P < 0.05$; **Figure 8C**). EGFR overexpression significantly increased cell viability

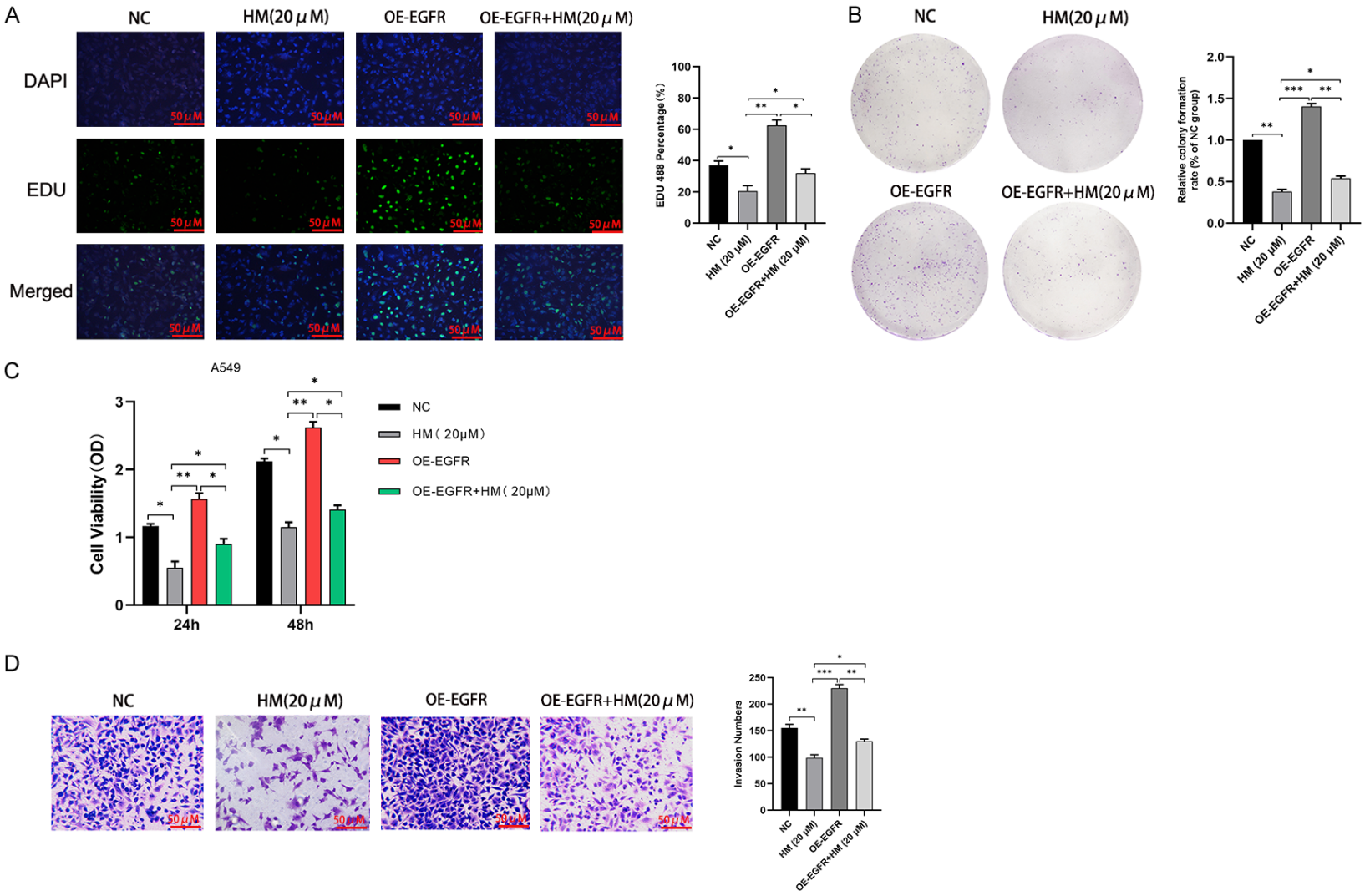
A
NC
HM(20 μM)
OE-EGFR
OE-EGFR+HM(20 μM)
DAPI
EDU
Merged
50 μM
EDU 488 Percentage (%)
NC
HM (20 μM)
OE-EGFR
OE-EGFR+HM (20 μM)
B
NC
HM(20 μM)
OE-EGFR
OE-EGFR+HM(20 μM)
Relative colony formation rate (% of NC group)
C
A549
Cell Viability (OD)
24h
48h
NC
HM（20μM）
OE-EGFR
OE-EGFR+HM（20μM）
D
NC
HM(20 μM)
OE-EGFR
OE-EGFR+HM(20 μM)
Invasion Numbers

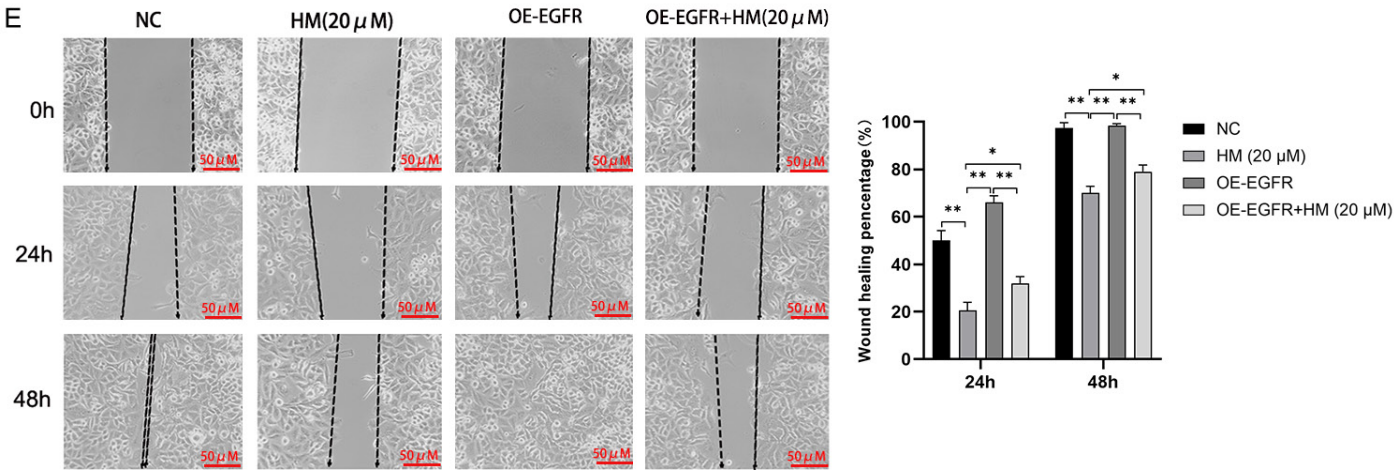

Figure 8. HM inhibits malignant behavior of human NSCLC A549 cells. A. EdU staining for cell proliferation detection. Scale bar = 50 μm. B. Colony formation assay for clonogenic capacity evaluation. C. CCK-8 assay showing cell viability of A549 cells treated with HM (20 μM) for 24 and 48 h. D. Transwell invasion assay. Scale bar = 50 μm. E. Wound healing assay for migration ability evaluation. Scale bar = 100 μm. Data are presented as mean ± SD from three independent experiments. *$P < 0.05$; **$P < 0.01$; ***$P < 0.001$.

compared with the NC group ($P < 0.01$). HM treatment also significantly reduced the viability of EGFR-overexpressing cells compared to the OE-EGFR group ($P < 0.01$), while the OE-EGFR+HM group remained significantly higher than the HM group ($P < 0.05$), further supporting the partial rescue effect.

The colony formation assay showed that HM significantly suppressed the clonogenic capacity of A549 cells compared to the NC group ($P < 0.01$; **Figure 8B**). EGFR overexpression promoted colony formation compared to the NC group ($P < 0.01$), whereas HM treatment significantly reduced colony formation in EGFR-overexpressing cells compared with the OE-EGFR group ($P < 0.05$). However, the colony number in the OE-EGFR+HM group remained significantly higher than that of the HM group ($P < 0.05$), confirming that EGFR overexpression partially rescued the clonogenic capacity in A549 cells.

Next, Transwell and wound healing assays were used to evaluate cell invasion and migration in A549 cells. HM significantly decreased the number of invading cells compared to the NC group ($P < 0.01$; **Figure 8D**), while EGFR overexpression significantly enhanced invasion compared to the NC group ($P < 0.01$). In the OE-EGFR+HM group, the number of invading cells was significantly lower than that of the OE-EGFR group ($P < 0.01$) but remained significantly higher than that in the HM group ($P < 0.05$). Similarly, wound healing assays showed that HM significantly reduced wound closure at 24 and 48 h compared to the NC group, whereas EGFR overexpression accelerated wound closure (**Figure 8E**). HM treatment significantly attenuated the EGFR overexpression-induced increase in migratory ability compared to the OE-EGFR group, while the OE-EGFR+HM group remained significantly higher than the HM group ($P < 0.05$).

Together, these results demonstrate that HM suppressed proliferation, colony formation, invasion, and migration of A549 cells. In all assays, EGFR overexpression significantly attenuated but did not abolish the inhibitory effects of HM, as evidenced by the consistent finding that OE-EGFR+HM group values were significantly higher than those of the HM group but significantly lower than those of the OE-EGFR group. These results confirm that the anti-malignant effects of HM are partially mediated through EGFR in A549 cells, consistent with the findings in LLC cells. Notably, in several assays, the OE-EGFR+HM group exhibited phenotypic levels even lower than those of the NC group, further underscoring the potent inhibitory activity of HM even under EGFR-overexpressing conditions. The similarity of these effects to those observed in LLC cells supports the generalizability of our findings beyond the murine model and suggests that HM may have therapeutic potential in human lung cancer.

HM promotes apoptosis of LLC cells in an EGFR-related manner

To further determine whether HM affects apoptosis in LLC cells, TUNEL staining, cleaved caspase-3 immunofluorescence, and western blotting were performed. As shown in **Figure 9A**, HM treatment significantly increased the proportion of TUNEL-positive cells compared with the NC group ($P < 0.01$) and significantly higher than that in the OE-EGFR group ($P < 0.01$), indicating enhanced apoptosis. EGFR overexpression partially reduced the HM-induced increase in TUNEL-positive cells ($P < 0.01$), suggesting that EGFR overexpression attenuated the pro-apoptotic effect of HM.

Consistent with the TUNEL results, immunofluorescence staining showed that HM markedly increased the proportion of cleaved caspase-3-positive cells compared with the NC group ($P < 0.001$; **Figure 9B**). EGFR overexpression alone did not significantly change cleaved caspase-3 expression. However, in the OE-EGFR+HM group, the percentage of cleaved caspase-3-positive cells was significantly lower than that of the HM group ($P < 0.001$) but remained significantly higher than that of the NC group ($P < 0.05$) and higher than that of the OE-EGFR group ($P < 0.01$), indicating that EGFR overexpression partially counteracted HM-induced caspase-3 activation.

Western blot analysis further confirmed these findings. HM increased cleaved caspase-3 protein expression, whereas EGFR overexpression attenuated this increase (**Figure 9C**). The cleaved caspase-3 level in the OE-EGFR+HM group was intermediate between the HM group and the OE-EGFR group, consistent with a partial rescue effect. Together, these results sug-

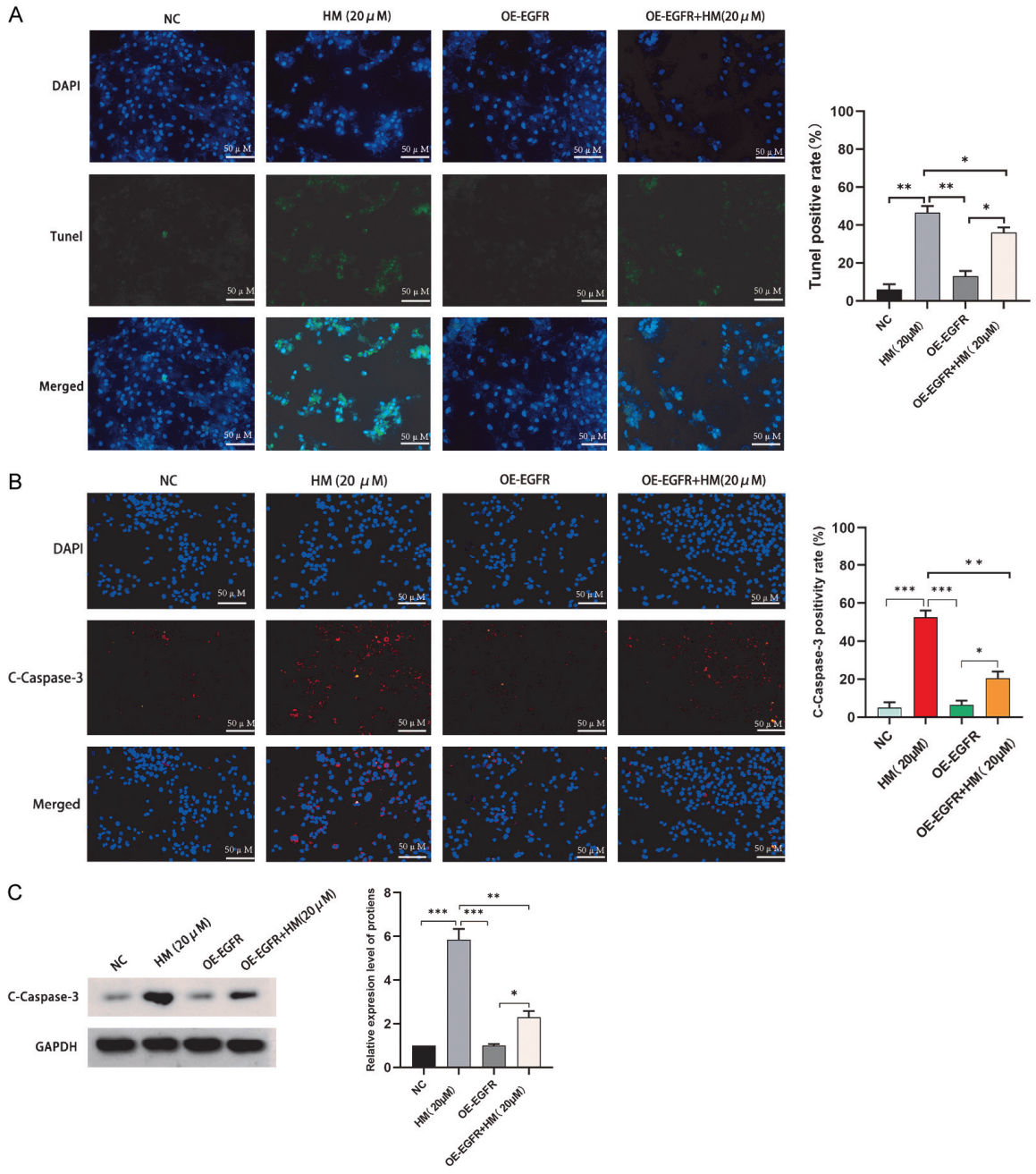

Figure 9. HM promotes apoptosis of LLC cells in an EGFR-related manner. A. TUNEL staining showing apoptotic cells after different treatments. Nuclei were counterstained with DAPI. Scale bar = 50 μm. Quantitative analysis of TUNEL-positive cells is shown on the right. B. Immunofluorescence staining of cleaved caspase-3 after different treatments. Nuclei were counterstained with DAPI. Scale bar = 50 μm. Quantitative analysis of cleaved caspase-3-positive cells is shown on the right. C. Western blot analysis of cleaved caspase-3 protein expression. GAPDH was used as the loading control. Data are presented as the mean ± SD from three independent experiments. *$P < 0.05$; **$P < 0.01$; ***$P < 0.001$.

gest that HM promotes apoptosis in LLC cells. EGFR overexpression partially attenuated HM-induced apoptosis, as indicated by the significant reduction in TUNEL-positive cells in the OE-EGFR+HM group compared to the HM group. However, the OE-EGFR+HM group still exhibited significantly higher apoptosis rates than the NC group, indicating that HM retains substantial pro-apoptotic activity even in the presence of EGFR overexpression. These find-

ings support the role of EGFR as a key mediator of HM-induced apoptosis while also suggesting the involvement of additional mechanisms.

Discussion

In this study, bioinformatics analysis, molecular docking, and in vitro functional assays were integrated to investigate the anti-tumor mechanism of HM in LLC cells. The results provide convergent evidence that HM suppresses several malignant phenotypes of LLC cells, including proliferation, colony formation, migration, and invasion, while promoting apoptosis. These effects were closely associated with inhibition of EGFR phosphorylation. Through target prediction and disease-gene mining, 121 overlapping targets between HM-related targets and LLC-related genes were identified. PPI network analysis further recognized EGFR as a candidate hub target. This finding is biologically plausible because EGFR is a well-established receptor tyrosine kinase involved in tumor cell proliferation, survival, migration, invasion, and therapeutic resistance. Recent studies have further highlighted the diverse roles of EGFR signaling in tumor biology, including kinase-dependent and kinase-independent regulation, EGFR-related ligand signaling, and abnormal receptor activation in malignant progression [38-40]. Functional enrichment analysis also supported the involvement of EGFR-related signaling, since the overlapping targets were enriched in biological processes related to protein phosphorylation and protein autophosphorylation, as well as in molecular functions associated with transmembrane receptor protein tyrosine kinase activity. These results provided a rationale for selecting EGFR for further mechanistic validation.

Molecular docking analysis offered a structural hypothesis for the potential interaction between HM and EGFR. HM was predicted to fit into the ATP-binding pocket of the EGFR kinase domain, with a binding energy below -7.0 kcal/mol. The predicted binding mode involved hydrophobic interactions, π-π stacking, and alkyl/π-alkyl interactions with residues within the EGFR active pocket. This suggests that HM may interfere with EGFR kinase activation. Previous structure-activity and pharmacological studies have shown that harmine and its derivatives possess anti-tumor potential and that structural modification of the β-carboline scaffold can influence their biological activity [41-43]. These reports support the plausibility that HM may interact with functionally relevant protein targets. Importantly, however, the docking result in the present study should still be interpreted as a computational prediction rather than definitive evidence of direct physical binding. Consistent with the docking prediction, cellular experiments showed that HM significantly reduced p-EGFR levels in LLC cells, whereas total EGFR expression was not significantly altered. This finding indicates that HM mainly suppresses EGFR activation by inhibiting its phosphorylation rather than by inducing EGFR protein degradation. Moreover, EGFR overexpression increased p-EGFR levels, while HM treatment partially reduced this increase. These findings link the structural prediction to a functional change in EGFR activation.

The functional assays further demonstrated that HM inhibited the malignant behaviors of LLC cells. CCK-8, EdU, and colony formation assays showed that HM reduced cell viability, DNA synthesis, and long-term clonogenic capacity. Transwell and wound healing assays showed that HM suppressed cell invasion and migration. In parallel, TUNEL staining, cleaved caspase-3 immunofluorescence, and western blotting showed that HM promoted apoptosis. These findings are generally consistent with previous evidence that HM can inhibit the growth of non-small cell lung cancer cells through mechanisms involving tumor cell death and growth suppression [44]. However, the present study extends previous observations by identifying EGFR phosphorylation as a key mechanistic event in LLC cells and by using EGFR overexpression to perform a rescue experiment. EGFR overexpression partially counteracted the effects of HM, including the inhibition of proliferation, migration, and invasion, as well as the induction of apoptosis. These rescue results suggest that EGFR-mediated signaling contributes to the anti-LLC activity of HM. The rescue effect was partial rather than complete. Therefore, HM may also act through additional targets or signaling pathways, which is consistent with the multi-target pharmacological characteristics of natural compounds.

Another relevant finding was that HM showed greater cytotoxicity toward LLC cells than toward BEAS-2B normal lung epithelial cells *in vitro*. This result supports the use of 20 μM HM in the subsequent functional assays and suggests preliminary tumor-selective cytotoxicity. Nevertheless, this conclusion should be interpreted cautiously because *in vitro* selectivity does not directly reflect in vivo safety, pharmacokinetics, or therapeutic efficacy. Several limitations should also be acknowledged. First, although molecular docking predicted a potential interaction between HM and EGFR, direct target engagement was not experimentally confirmed. Surface plasmon resonance, cellular thermal shift assay, drug affinity responsive target stability assay, or pull-down experiments would be needed to verify direct physical binding. Second, this study combines a human EGFR structure for docking and mouse LLC cells for functional experiments. Regarding the species discrepancy between docking and cellular validation, human and mouse EGFR share approximately 90% amino acid identity in the kinase domain, and the ATP-binding pocket residues critical for inhibitor binding are fully conserved between the two species, supporting the use of the human EGFR crystal structure in the context of mouse LLC cells. Nevertheless, minor sequence differences outside the pocket cannot be excluded, and cross-species findings should be interpreted with caution. The consistency of HM's effects in human A549 cells partially addresses this concern, but further validation in additional human cell lines and in vivo models is warranted. Third, the disease-associated genes used for bioinformatics analysis were originally derived from human databases; these genes were converted to mouse orthologs using the biomaRt R package. Although this is a standard and widely accepted approach in cross-species bioinformatics analyses, minor mapping biases cannot be completely excluded, and the bioinformatics-based findings should be interpreted with this consideration. Future studies should further clarify these signaling events and evaluate the pharmacological properties, toxicity profile, and potential combination effects of HM with existing EGFR inhibitors.

Conclusion

This study suggested that HM suppresses the malignant phenotypes of LLC cells, at least in part, by inhibiting EGFR phosphorylation and EGFR-mediated signaling. EGFR serves as an important candidate target that links the bioinformatic prediction, molecular docking analysis, and cellular functional validation. These findings provide mechanistic insight into the anti-tumor activity of HM and support further preclinical investigation of HM as a candidate compound for lung cancer therapy.

Acknowledgements

This work was supported by the following grants: 1. The Natural Science Foundation of Gansu Province [Grant Number 23JRRA1801]; 2. The Gansu Provincial Health and Medical Research Program [Grant Number GSWSKY-2020-04]; 3. The Key Research and Development Project of Gansu Province Science and Technology Plan (22YF7FA099); 4. The Lanzhou Municipal Science and Technology Programme (2022-3-39); 5. Healthcare Service and Security Enhancement Fund (10000015Z155080000004).

Disclosure of conflict of interest

None.

Address correspondence to: Ruoyu Zhao, Department of Gastrointestinal Medical Oncology, Sun Yat-sen University Cancer Center Gansu Hospital and Gansu Provincial Cancer Hospital, Lanzhou 730050, Gansu, China. E-mail: zhaoruoyu@163.com

References

[1] Bray F, Laversanne M, Sung H, Ferlay J, Siegel RL, Soerjomataram I and Jemal A. Global cancer statistics 2022: GLOBOCAN estimates of incidence and mortality worldwide for 36 cancers in 185 countries. CA Cancer J Clin 2024; 74: 229-263.

[2] Siegel RL, Giaquinto AN and Jemal A. Cancer statistics, 2024. CA Cancer J Clin 2024; 74: 12-49.

[3] Yamada-Hara M, Takahashi N, Byun JW, Zeng L, Wang Z, Tanaka A, Malakoutikhah Z, Hayashi T, Webster NJG, Raz E and Bertin S. In vivo bioluminescence imaging of tumor progression in the Lewis lung carcinoma orthotopic mouse model: a comparison between the tail vein injection and intranasal instillation methods. Curr Protoc 2024; 4: e70071.

[4] Li S, Wang A, Gu F, Wang Z, Tian C, Qian Z, Tang L and Gu Y. Novel harmine derivatives for tumor targeted therapy. Oncotarget 2015; 6: 8988-9001.

[5] Liu Q, Yang C, Qi J, Shen Q, Ye M, Li H and Zhang L. Bioactivities and structure-activity relationships of harmine and its derivatives: a review. Chem Biodivers 2025; 22: e202402953.
[6] Sarkar S, Tribedi P and Bhadra K. Structure-activity insights of harmine targeting DNA, ROS inducing cytotoxicity with PARP mediated apoptosis against cervical cancer, anti-biofilm formation and *in vivo* therapeutic study. J Biomol Struct Dyn 2022; 40: 5880-5902.
[7] Zhang L, Li D and Yu S. Pharmacological effects of harmine and its derivatives: a review. Arch Pharm Res 2020; 43: 1259-1275.
[8] Yu L, Bi K, Gu J, Yu Z, Li S and Chen Y. Harmine exerts anticancer effects through the ROS/p38 axis to induce autophagy and apoptosis in osteosarcoma. Bioorg Chem 2025; 161: 108557.
[9] Liu FH, Lin XC, Liu YW, Zhang TT, Zhang YB, Xie ZL, Zhan Y and Hu P. Harmine inhibits the proliferation and migration and promotes the apoptosis of colon cancer cells via inhibition of the FAK/AKT and ERK(1/2)/CREB signaling pathways. J Asian Nat Prod Res 2025; 27: 75-87.
[10] Cho CC, Lin CJ, Huang HH, Yang WZ, Fei CY, Lin HY, Lee MS and Yuan HS. Mechanistic insights into harmine-mediated inhibition of human DNA methyltransferases and prostate cancer cell growth. ACS Chem Biol 2023; 18: 1335-1350.
[11] Zhai Y, Chen K, Xu Z, Chen X, Tong J, He Y, Chen C, Ding M, Liang G and Zheng X. Harmine alleviates LPS-induced acute lung injury by inhibiting CSF3-mediated MAPK/NF-κB signaling pathway. Respir Res 2025; 26: 119.
[12] Hai-Rong C, Xiang H and Xiao-Rong Z. Harmine suppresses bladder tumor growth by suppressing vascular endothelial growth factor receptor 2-mediated angiogenesis. Biosci Rep 2019; 39: BSR20190155.
[13] Zheng ZH, Lin XC, Lu Y, Cao SR, Liu XK, Lin D, Yang FH, Zhang YB, Tu JL, Pan BX, Hu P and Zhang WH. Harmine exerts anxiolytic effects by regulating neuroinflammation and neuronal plasticity in the basolateral amygdala. Int Immunopharmacol 2023; 119: 110208.
[14] Ock CW and Kim GD. Harmine hydrochloride mediates the induction of G2/M cell cycle arrest in breast cancer cells by regulating the MAPKs and AKT/FOXO3a signaling pathways. Molecules 2021; 26: 6714.
[15] Uhl KL, Schultz CR, Geerts D and Bachmann AS. Harmine, a dual-specificity tyrosine phosphorylation-regulated kinase (DYRK) inhibitor induces caspase-mediated apoptosis in neuroblastoma. Cancer Cell Int 2018; 18: 82.
[16] Bao Y, Zhu J, Mao X, Zhang M, Ao Q, Zhu H and Gao J. Harmine inhibits ovarian cancer migration and invasion and epithelial-mesenchymal transition (EMT) by inhibiting HDAC7 to restore RECK expression. Biochem Pharmacol 2025; 242: 117391.
[17] Jalali A, Dabaghian F and Zarshenas MM. Alkaloids of *Peganum harmala*: anticancer biomarkers with promising outcomes. Curr Pharm Des 2021; 27: 185-196.
[18] Kim GD. Harmine hydrochloride induces G2/M cell cycle arrest and apoptosis in SK-Hep1 hepatocellular carcinoma cells by regulating mitogen-activated protein kinases and the PI3K/AKT pathway. Prev Nutr Food Sci 2023; 28: 436-443.
[19] Tshikhudo PP, Mabhaudhi T, Koorbanally NA, Mudau FN, Avendaño Caceres EO, Popa D, Calina D and Sharifi-Rad J. Anticancer potential of β-carboline alkaloids: an updated mechanistic overview. Chem Biodivers 2024; 21: e202301263.
[20] Gekle M, Dubourg V, Schwerdt G, Benndorf RA and Schreier B. The role of EGFR in vascular AT1R signaling: from cellular mechanisms to systemic relevance. Biochem Pharmacol 2023; 217: 115837.
[21] Roberts PJ and Der CJ. Targeting the Raf-MEK-ERK mitogen-activated protein kinase cascade for the treatment of cancer. Oncogene 2007; 26: 3291-3310.
[22] Zinatizadeh MR, Miri SR, Zarandi PK, Chalbatani GM, Rapôso C, Mirzaei HR, Akbari ME and Mahmoodzadeh H. The hippo tumor suppressor pathway (YAP/TAZ/TEAD/MST/LATS) and EGFR-RAS-RAF-MEK in cancer metastasis. Genes Dis 2019; 8: 48-60.
[23] Fitzgerald TL, Lertpiriyapong K, Cocco L, Martelli AM, Libra M, Candido S, Montalto G, Cervello M, Steelman L, Abrams SL and McCubrey JA. Roles of EGFR and KRAS and their downstream signaling pathways in pancreatic cancer and pancreatic cancer stem cells. Adv Biol Regul 2015; 59: 65-81.
[24] Bang J, Jun M, Lee S, Moon H and Ro SW. Targeting EGFR/PI3K/AKT/mTOR signaling in hepatocellular carcinoma. Pharmaceutics 2023; 15: 2130.
[25] de Kort WWB, Spelier S, Devriese LA, van Es RJJ and Willems SM. Predictive value of EGFR-PI3K-AKT-mTOR-pathway inhibitor biomarkers for head and neck squamous cell carcinoma: a systematic review. Mol Diagn Ther 2021; 25: 123-136.
[26] Singh G, Rohit, Kumar P and Aran KR. Targeting EGFR and PI3K/mTOR pathways in glioblastoma: innovative therapeutic approaches. Med Oncol 2025; 42: 97.

[27] Levantini E, Maroni G, Del Re M and Tenen DG. EGFR signaling pathway as therapeutic target in human cancers. Semin Cancer Biol 2022; 85: 253-275.
[28] Kumagai S, Koyama S and Nishikawa H. Antitumour immunity regulated by aberrant ERBB family signalling. Nat Rev Cancer 2021; 21: 181-197.
[29] Kang X, Li R, Li X and Xu X. EGFR mutations and abnormal trafficking in cancers. Mol Biol Rep 2024; 51: 924.
[30] Sabbah DA, Hajjo R and Sweidan K. Review on epidermal growth factor receptor (EGFR) structure, signaling pathways, interactions, and recent updates of EGFR inhibitors. Curr Top Med Chem 2020; 20: 815-834.
[31] Araki T, Kanda S, Horinouchi H and Ohe Y. Current treatment strategies for EGFR-mutated non-small cell lung cancer: from first line to beyond osimertinib resistance. Jpn J Clin Oncol 2023; 53: 547-561.
[32] Girard N. EGFR-mutated NSCLC: a roadmap to treatment sequences. Med 2024; 5: 1044-1047.
[33] Zhang D, Zhao J, Yang Y, Dai Q, Zhang N, Mi Z, Hu Q and Liu X. Fourth-generation EGFR-TKI to overcome C797S mutation: past, present, and future. J Enzyme Inhib Med Chem 2025; 40: 2481392.
[34] Kashizaki F, Chen H, Miyasaka A, Tsuchiya N, Yamada C, Okazaki S, Kaneko M, Kano T, Kameda Y, Kikuchi A, Yumoto K, Osawa H, Koizumi H, Takahashi K and Kaneko T. Safety of readministration of EGFR-TKI after onset of interstitial lung disease in advanced EGFR-mutated NSCLC: a systematic review and meta-analysis. Clin Lung Cancer 2024; 25: e52-e57, e2.
[35] Malapelle U, Pilotto S, Passiglia F, Pepe F, Pisapia P, Righi L, Listì A, Bironzo P, Belluomini L, Tabbò F, Reale ML, Russo G, De Luca C, Novello S and Troncone G. Dealing with NSCLC EGFR mutation testing and treatment: a comprehensive review with an Italian real-world perspective. Crit Rev Oncol Hematol 2021; 160: 103300.
[36] Zhao Y, Wang H and He C. Drug resistance of targeted therapy for advanced non-small cell lung cancer harbored EGFR mutation: from mechanism analysis to clinical strategy. J Cancer Res Clin Oncol 2021; 147: 3653-3664.
[37] Hassanein SS, Ibrahim SA and Abdel-Mawgood AL. Cell behavior of non-small cell lung cancer is at EGFR and MicroRNAs hands. Int J Mol Sci 2021; 22: 12496.
[38] He X, Wang QX, Wei D, Lin Y, Zhang X, Wu Y, Qian X, Lin Z, Xiao B, Wu Q, Wang Z, Zhou F, Wei Z, Wang J, Gong R, Zhang R, Zhang Q, Ding K, Gao S and Kang T. Lysosomal EGFR acts as a Rheb-GEF independent of its kinase activity to activate mTORC1. Cell Res 2025; 35: 497-509.
[39] Cheng WL, Feng PH, Lee KY, Chen KY, Sun WL, Van Hiep N, Luo CS and Wu SM. The role of EREG/EGFR pathway in tumor progression. Int J Mol Sci 2021; 22: 12828.
[40] Yi SA, Cho D, Kim S, Kim H, Choi MK, Choi HS, Shin S, Yun S, Lim A, Jeong JK, Yoon DE, Cha HJ, Kim K, Han JW, Cho HS and Cho J. Functional loss of ERBB receptor feedback inhibitor 1 (MIG6) promotes glioblastoma tumorigenesis by aberrant activation of epidermal growth factor receptor (EGFR). Mol Oncol 2025; 19: 937-953.
[41] Akabli T, Toufik H and Lamchouri F. *In silico* modeling studies of *N(9)*-substituted harmine derivatives as potential anticancer agents: combination of ligand-based and structure-based approaches. J Biomol Struct Dyn 2022; 40: 3965-3978.
[42] Cao R, Fan W, Guo L, Ma Q, Zhang G, Li J, Chen X, Ren Z and Qiu L. Synthesis and structure-activity relationships of harmine derivatives as potential antitumor agents. Eur J Med Chem 2013; 60: 135-143.
[43] Patel K, Gadewar M, Tripathi R, Prasad SK and Patel DK. A review on medicinal importance, pharmacological activity and bioanalytical aspects of beta-carboline alkaloid 'Harmine'. Asian Pac J Trop Biomed 2012; 2: 660-664.
[44] He J, Xiong Q, Qi Y, Peng C, Hu L, Xia M, Zhu B, Xu B and Ding Y. Harmine inhibits non-small cell lung cancer growth by targeting phosphodiesterase4D and inducing ferroptosis. Phytomedicine 2026; 150: 157640.